Cite this: *Soft Matter*, 2011, **7**, 4938

www.rsc.org/softmatter

PAPER

Planar lamellae and onions: a spatially resolved rheo–NMR approach to the shear-induced structural transformations in a surfactant model system

Bruno Medronho,[ac] Jennifer Brown,[be] Maria Graça Miguel,[a] Claudia Schmidt,[d] Ulf Olsson[c] and Petrik Galvosas*[e]

Received 16th November 2010, Accepted 7th March 2011
DOI: 10.1039/c0sm01323d

The shear-induced transformations between oriented planar lamellae and a state of closely packed multilamellar vesicles (MLVs) in a lyotropic nonionic surfactant model system were studied by the combination of nuclear magnetic resonance (NMR) spectroscopy and diffusometry with magnetic resonance imaging (MRI). ^{2}H NMR imaging confirmed the discontinuous nature of the transition from onions to planar lamellae, revealing the spatial coexistence of both states within the gap of the cylindrical Couette geometry. On the other hand, NMR diffusion measurements in three principal directions and at various values of strain strongly suggest that a multi-lamellar cylindrical or undulated intermediate structure exists during the continuous and spatially homogeneous transition from planar lamellae to MLVs.

1. Introduction

The lyotropic lamellar (L_α) phase is well known for its complex response to shear flow. When shear is applied at a constant rate the equilibrium L_α structure consisting of extended stacks of bilayers may be transformed to a particular defect structure resembling close-packed multilamellar vesicles (MLVs). This phenomenon was first investigated in detail by Roux and collaborators.[1–4] The MLVs, also know as onions or spherulites, are fairly monodisperse in size with a radius in the range from hundreds of nanometres to tens of micrometres that is tunable by the applied shear rate.

Due to their amphiphilic constituents the surfactant bilayers form a barrier to both hydrophilic and hydrophobic molecules. Therefore MLVs, which are metastable and may persist for long times, are investigated as possible containers and delivery systems for drugs and nanoparticles.[5–14] They also show potential as microreactors.[15,16]

The initial formation of the onion structure from the "normal" L_α phase is accompanied by an increase in viscosity. However, once the onions have been formed, the system becomes shear-thinning and the viscosity decreases as the onion radius R_{MLV} becomes smaller with increasing shear rate, often following a power law, $R_{MLV} \propto \dot{\gamma}^{-a}$, with $a \approx 0.5$.[2,17] Periodic structures may be formed due to the low MLV polydispersity.[18–23] Electron microscopy shows there are no solvent-filled voids in the system. Space is completely filled by the lamellar phase and the onions have polyhedral shapes.[24]

Shear-induced MLVs have been found in many L_α phases,[25–29] independent of the type of surfactant used. They have been observed in systems containing anionic,[1–4,19,30–39] cationic,[40–43] nonionic[17,23,44–49] or mixed cationic/anionic surfactants[50] as well as in lamellar phases formed by polymeric surfactants of the block copolymer[51–53] or the side-chain polymer type.[54,55] They occur in simple binary systems,[17,44–49] in surfactant/water systems with additional cosurfactant and/or salt[1,19,30–32,34–36,38,39] and in multi-component oil-swollen systems.[2–4,30,33,37]

The stability regions of both planar lamellae and MLVs as a function of shear rate and temperature can be readily obtained from, for instance, the ^{2}H NMR line shapes of D_2O-enriched samples[17,44] and mapped in a so called orientation or shear diagram.[2,56] Moreover, transient processes under shear flow, such as the formation of MLVs from initially planar lamellae (lamellae-to-onion) or the reverse transformation (onion-to-lamellae) can be followed by time-dependent ^{2}H NMR experiments.[57] The shear-induced transitions in surfactant systems may be continuous or discontinuous.[4,58] In a previous work, while using a well-documented nonionic surfactant model system composed of 40 wt% of triethylene glycol mono n-decyl ether ($C_{10}E_3$) in water,[46,56,57,59–70] a fundamental difference in mechanism was found when comparing the transition from planar lamellae to MLVs with the opposite transition, from MLVs to planar lamellae.[57]

In $C_{10}E_3$/water (40 wt%), onions occur only below a certain temperature at sufficiently high shear rates.[56] At higher

[a]*Department of Chemistry, University of Coimbra, 3004-535 Coimbra, Portugal*
[b]*Chemical and Biological Engineering, Montana State University, 306 Cobleigh Hall, PO Box 173920, Bozeman, MT, 59717-3920, USA*
[c]*Physical Chemistry 1, Center of Chemistry and Chemical Engineering, Lund University, Box 124, 221 00 Lund, Sweden*
[d]*Department of Chemistry, University of Paderborn, Warburger Str. 100, D-33098 Paderborn, Germany*
[e]*MacDiarmid Institute for Advanced Materials and Nanotechnology, School of Chemical and Physical Sciences, Victoria University of Wellington, PO Box 600, Wellington, New Zealand. E-mail: petrik.galvosas@vuw.ac.nz*

temperatures the application of shear leads to aligned layers whose normal is parallel to the velocity gradient ("gradient" will refer to the gradient in velocity of the flow field, not to the "magnetic field gradient" used elsewhere in this paper). Thus, by a proper choice of shear rate and temperature a well-defined initial state of either aligned layers or onions can be prepared. Subsequently, after a change of shear rate and/or temperature, the temporal evolution to the other state can be studied.[57] Our investigation by means of ^{2}H NMR spectroscopy has shown that the lamellae-to-onion transition is a continuous process with a homogeneous generation of defects throughout the sample until the steady state of the fully developed onion structure is reached. On the other hand, when shear rates and temperatures outside the metastable regime for onions are applied to the onion state, the shear-induced transformation of the onions back to aligned layers is heterogeneous and goes through a regime of two coexisting states, resembling a nucleation-and-growth process.

These previous experiments have not allowed us to determine whether domains of aligned layers start to grow from different locations in the sample or whether there is a preferred nucleation site, for example, at the boundaries of the shear cell. In this contribution, we answer this question by means of spatially-resolved ^{2}H NMR spectroscopy[71,72] (^{2}H NMR imaging) as well as spatially-resolved pulsed magnetic field gradient NMR diffusometry[73,74] (diffusion imaging). The large anisotropy of the diffusion tensor in the lamellar phase makes NMR diffusometry a useful tool for probing structural details of the lamellar phase.[75–80]

A second question, which can also be tackled by means of NMR diffusometry, concerns the pathway of onion formation from the aligned L_α phase. Despite the large number of investigations it still remains a puzzle how onions are actually formed from extended stacks of planar bilayers. The formation of an intermediate structure of multilamellar cylinders was suggested by Zipfel, Nettesheim and collaborators.[59,60] During the transition from the aligned lamellar state to onions, they found a reproducible intermittent plateau in the curve of increasing viscosity measured as a function of strain. Scattering experiments carried out on this intermediate state are consistent with a structure of multilamellar cylinders aligned along the velocity direction. Here, we will report on NMR diffusion experiments which may shed more light on this intermediate structure and the process of onion formation.

The outline of this paper is as follows: in the experimental section, after a short description of the sample preparation and the experimental setup, the fundamentals of the ^{2}H NMR imaging and diffusion imaging will be presented. The subsequent results and discussion section consists of two parts. First we study the spatial dependence of both the lamellae-to-onion and the reverse transition investigated by ^{2}H imaging as well as diffusion imaging. Second we report on the existence of an intermediate structure during the lamellae-to-onion transition as obtained by diffusion imaging.

2. Experimental

2.1 Surfactant system

$C_{10}E_3$ with a purity higher than 99.8% was purchased from Nikko Chemical Co. (Tokyo, Japan). Deuterium oxide (D_2O) was obtained from Sigma Chemicals (Steinheim, Germany). Samples containing 40 wt% surfactant were prepared by weighing the desired amounts of surfactant and water into vials, mixing and centrifuging them in order to remove air bubbles. All samples were prepared with a ratio D_2O/H_2O of 9 : 1 by weight.

2.2 Rheo–NMR devices and NMR apparatus

For all experiments, concentric cylinder rheo–NMR Couette devices were used, as depicted in Fig. 1 (left part).

Two shear cells were constructed of standard glass NMR tubes. The inner rotating tubes had diameters of 16 mm and 20 mm and rested inside the outer stationary tubes of diameter 18 mm and 23 mm, resulting in fluid gap widths of 1 mm and 1.5 mm, respectively. Teflon spacers in the gap between cylinders ensure concentricity and smooth rotation of the inner cylinder. The sample is placed in the gap between the two tubes. The outer, stationary tube is held by the NMR coil assembly while the inner tube is turned by a stepper motor *via* a gear box and a rigid mechanical drive shaft.[81] The stepper motor is able to apply rotations in the frequency range 0.1 Hz to 14 Hz. Two gear boxes with the ratios 25 : 2 and 50 : 1 were utilized to access shear rates of interest for the different experiments. These gap-average shear rates were calculated according to the following equation[82]

$$\dot{\gamma} = \frac{r_i \omega_i}{r_o - r_i} \quad (1)$$

valid for small gap sizes. The radii of the outer and inner cylinders are r_o and r_i, respectively, while ω_i is the inner cylinder angular velocity.

Two Avance spectrometers (Bruker) have been used, both operating at a ^{1}H resonance frequency of 400 MHz. A Bruker Micro2.5 three-axes micro-imaging system provided magnetic field gradients of up to 1.45 T m^{-1} for imaging as well as diffusion encoding.

2.3 NMR imaging

NMR imaging is used for the acquisition of spatially resolved ^{2}H quadrupole splittings (as a measure of molecular order) as well as diffusion coefficients in the three principal directions (as a measure of anisotropy). This research is as much about the NMR methodology as it is about the rheological properties of

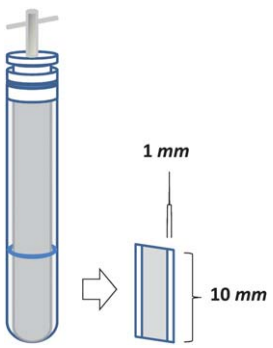

Fig. 1 Schematic illustration of the Couette geometry used (left). The right figure depicts the active sample volume (white strips in the slice) after double slice selection in the diffusometry experiments.

the surfactant system. We therefore will provide experimental details for both methods used in this subsection. However, the rheology results in section 3 stand on their own and may be interpreted without going into the details of the NMR experiments.

2.3.1 ^{2}H NMR imaging. Molecular ordering in complex systems can be monitored through the ^{2}H NMR spectra of D_2O-enriched samples, where the quadrupolar interaction produces a peak splitting proportional to the local order.[83] Spatially resolved spectra across the fluid gap may be obtained by means of ^{2}H NMR imaging[71,72] for samples prepared with D_2O.

One-dimensional (1D) NMR images containing the spectroscopic information in each pixel of the image were acquired. Due to the fast T_2 relaxation of the MLVs (5 ms), the NMR signal must be acquired fairly quickly after the initial excitation, making the short pulse sequence shown in Fig. 2 an attractive option for acquisition of 1D ^{2}H NMR images. In addition the use of phase encoding retains spectral information. The Couette cell, depicted in Fig. 1, is a three dimensional object. However, by shifting the curved cell bottom outside of the active region of the rf-resonator, the acquired signal is invariant along the vorticial direction (z), reducing the spatial dimensionality to a 2D cross-sectional annulus in plane perpendicular to the z-direction. The sequence in Fig. 2 acquires a projection of this 2D annulus onto a line in the x,y-plane *via* application of a phase encoding magnetic field gradient in the x-direction prior to signal acquisition. The experiment produces two-dimensional data files with 1024 acquisition points in the time domain (FID) and 128 points in k-space.[73,84] Fourier transformation (FT) of the time domain signal yields the deuterium spectra (frequency domain) while FT of the k-direction yields the said projection with a resolution of approximately 161 μm pixel^{-1} (20 mm field of view). Such a spatial resolution permits around 6 pixels across the annular gap of the Couette cell. A total of 4 scans were acquired for each k-space magnetic field gradient step.

To extract the desired 1D ^{2}H NMR image, the obtained 1D projection may be subjected to an inverse Abel transformation (IAT) because of the cylindrical symmetry of the object.[85] The resulting ^{2}H NMR image (1D in space) contains the desired spatially resolved spectral information in dependency on the distance to the axis of rotation. One could, in principle, apply the so called Hankel transformation (HT) directly to the k-space data and obtain the wanted ^{2}H NMR image. However, we followed the approach of Major *et al.*[85] to use the FT first as this allows for a baseline correction and the centering of the projection profile which ensures cylindrical symmetry. For the final step in the data processing we did not use, in contrast to Major *et al.*,[85] the IAT, as we found this transformation susceptible to experimental noise because of the first derivative of the projection profile used in this transformation.[85] Instead, we used the inverse FT, transforming the corrected data back into k-space and applied the HT subsequently. One example of the result of this procedure is represented in Fig. 3. On the top part of the figure, we can observe the spectrum of a planar lamellar phase at 36 °C in the frequency domain (cut represented by the horizontal dashed line) while on the lateral right side of Fig. 3, the 1D profile across the cell with peaks indicating the position of the annular gap is demonstrated (cut represented by the vertical dashed line).

^{2}H NMR imaging was used for the investigation of the transition from the lamellar state to MLVs by placing the filled Couette cell in the micro-imaging probe and setting the sample temperature to 42 °C. A shear rate of 5 s^{-1} was applied for 60 min. Under such conditions the expected structure is a lamellar phase in the c-orientation (also called parallel orientation, layer normal parallel to the velocity gradient, here perpendicular to the static magnetic field). Once the c-orientation was achieved, shear was stopped and temperature decreased to 36 °C. Strain ($\gamma = \dot{\gamma}t$) was applied in several steps ("start–stop" experiment) to complete the transition using a constant shear rate of 5 s^{-1}. Five initial steps of $\gamma = 600$ (each step took 120 s) were applied, followed by one step with $\gamma = 6000$ (20 min) and a final step of $\gamma = 27000$ (90 min), resulting in a total strain of 36000. After each strain step, a ^{2}H NMR image, containing the spatially resolved quadrupole splitting, was taken over a period of about 25 min.

For the opposite transition we prepared MLVs initially at 36 °C with a constant shear rate of 5 s^{-1} during 1 h. Then, shear was ceased and temperature increased to 42 °C. Several strain

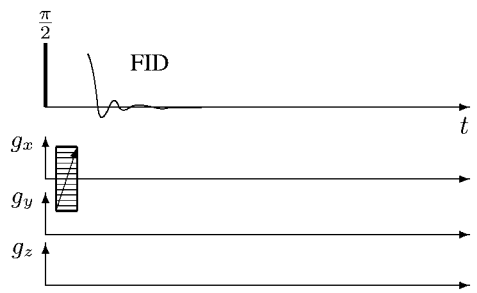

Fig. 2 Rf and magnetic field gradient pulse sequences for ^{2}H NMR imaging. The 1D image is purely phase encoded in x-direction.

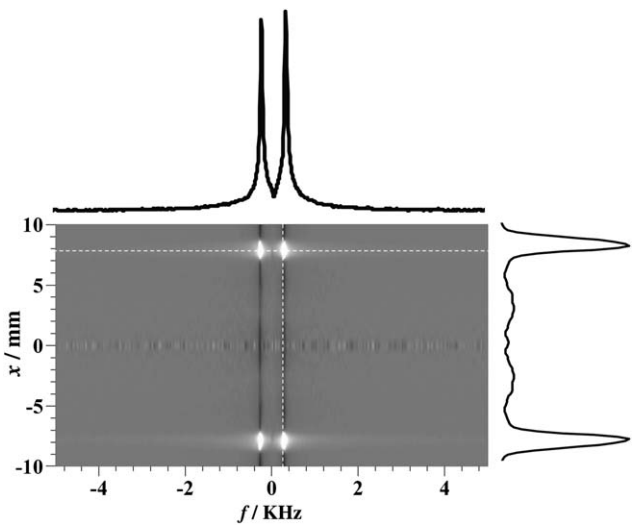

Fig. 3 Example of data processing for ^{2}H NMR imaging: both an example of the spectrum (insert on top) and a 1D profile across the Couette cell (insert on the right side) are represented corresponding to the horizontal and vertical cuts (dashed lines), respectively.

steps (at a shear rate of 0.5 s^{-1}) were applied to complete the transition from MLVs to planar lamellae, starting with five steps of 30 strain units each (each step took 60 s). This was followed by one step of $\gamma = 50$, three steps of $\gamma = 100$, one step of $\gamma = 400$ and a final step of $\gamma = 900$, resulting in a total strain of 1800. In between each strain step, and as done for the lamellae-to-onion transition, ^{2}H NMR imaging experiments were performed.

2.3.2 Diffusion imaging. Diffusion imaging was performed based on the reasonable assumption that the water self-diffusion coefficient, D_w, in the different spatial directions, should depend on the surrounding structure and spatial orientation in which the water is diffusing. For ideal planar lamellae oriented as shown in Fig. 4 with the layers parallel to the walls of the Couette cell, D_w is expected to be "free" in the vorticity and velocity directions and restricted along the velocity gradient direction. On the other hand, one should not expect any spatial dependence of D_w for MLVs. In contrast, a cylinder-like intermediate should give rise to a different distinct diffusion behavior again. In this case, D_w is expected to be "free" along the cylinder axis and restricted in the remaining spatial directions.

The pulse sequence used for the diffusion imaging is shown in Fig. 5 and incorporates a standard pulsed gradient stimulated echo (PGSTE) sequence with frequency encoding to obtain 1D images at proton resonance frequency and slice selection in two dimensions.[86] In the PGSTE sequence, a pair of trapezoidal narrow magnetic field gradient pulses with amplitude g (in either the x, y or z-direction) and duration δ (set to 10 ms) encode for spin displacement over a controlled observation time Δ (set to 20 ms). After the initial $\pi/2$ rf excitation pulse, the first pulsed magnetic field gradient is applied during the transverse evolution delay τ_1, imparting a phase shift dependent upon position. In a stimulated echo sequence, a second $\pi/2$ rf pulse stores the magnetization along z during τ_2, where it is subject only to T_1 and not to T_2 relaxation. A third $\pi/2$ rf pulse brings the magnetization back into the transverse plane, and in

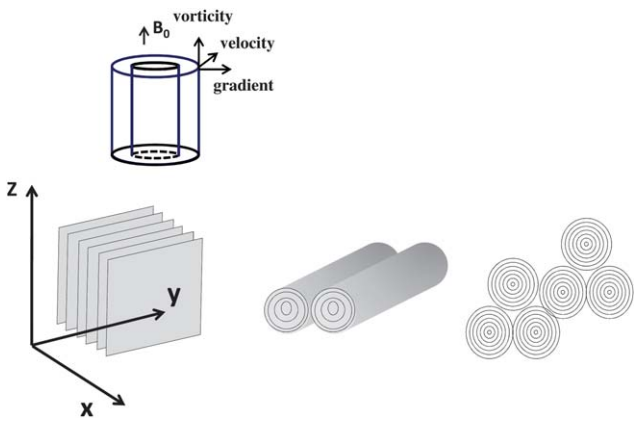

Fig. 4 Possible lamellae topologies and their orientation in the laboratory frame (from left to right): planar lamellae (in the so called c-direction), multilayered cylinders and MLVs. Note that x, y, and z refer to the pulsed magnetic field gradients as used in the diffusion imaging experiments. With respect to the shear frame (see schematic Couette cell on top), x, y and z correspond to the velocity gradient, velocity and vorticity directions, respectively.

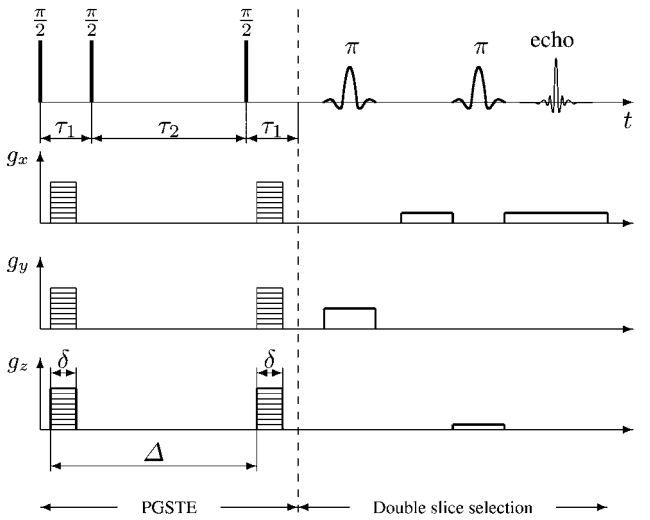

Fig. 5 Rf and magnetic field gradient pulse sequences for diffusion imaging. Two magnetic field gradient pulses of duration δ and separation Δ are applied in either x, y or z-direction and increased successively in amplitude. Two soft 180° pulses are used complementary in combination with magnetic field slice gradients in the y and z-direction to select a specific volume of spins.

combination with the second pulsed magnetic field gradient causes the signal to re-phase. Any residual phase shift in the signal is due to motion of the spins from their original position. Diffusive motion causes a phase spread that results in attenuation of the echo signal, which when fitted with the Stejskal–Tanner equation[87]

$$E = E_0 \exp\left\{-D(\gamma\delta g)^2\left(\Delta - \frac{1}{3}\delta\right)\right\} = E_0 e^{-Db} \qquad (2)$$

yields the diffusion coefficient D. γ is the gyromagnetic ratio and E_0 the signal amplitude without pulsed magnetic field gradients applied. It is convenient to introduce the so called b-factor, as given by eqn (2), which represents all parameters controlled by the experiment.

Due to the cylindrical symmetry of the Couette cell, double slice selection was adopted in order to measure and distinguish directional diffusivities in the sample under study. By applying the pulsed magnetic field gradients in either the x, y or z-direction the corresponding diffusion coefficient can be determined (while the sample is under rest) and assigned to either the velocity, velocity gradient or vorticity axes in the shear frame as explained by Callaghan.[81] After application of the magnetic field gradient pair, a π rf soft pulse is applied in conjunction with a magnetic field gradient in the y-direction to select only spins in a slice in the x,z-plane with a thickness $\Delta y = 1$ mm. This slice is positioned across the center of the cell selecting two opposite strips from the annular gap. A second π soft pulse, applied simultaneously with a magnetic field gradient in the z-direction, selects spins further in a slice of thickness $\Delta z = 10$ mm transverse to the first one so that the signal comes from a small fraction of the total sample. This double slice selection scheme ensures that the NMR signal emerges only from a subsection of the sample with negligible curvature. Fig. 1 (right part) schematically illustrates the selected volume of spins (two white strips). The NMR echo is then

acquired under the influence of a magnetic field gradient which allows one to obtain 1D profiles across the cell. The data files are two-dimensional with 512 points in the time domain (echo) and 8 points in q-space.[73,84] A total of 4 scans were acquired for each q-space magnetic field gradient step. Note that the pulse sequence does neither allow the simultaneous measurement of D_w in the gradient, velocity and vorticity directions independently nor the measurement under shear. Hence, the start–stop experimental protocol was adopted.

Fig. 6 and Fig. 7 exemplify how D_w regardless of the direction of the diffusive process was extracted; 1D Fourier transformation of the time domain data (the echo) lead to a 1D intensity profile across the geometry of the Couette cell for each value of the applied magnetic field q-gradient (Fig. 6).

Subsequent integration of the intensities across the gap yield NMR signal amplitudes for each of the pulsed magnetic field q-gradients applied. D_w was extracted by fitting the spin echo attenuation *versus* b as given by eqn (2) and as shown in Fig. 7. Note that each individual diffusion experiment in any of the spatial directions took approximately 10 min (for 8 magnetic field q-gradient steps and 4 scans). Therefore, there were intervals of approximately 30 min between each strain value. Increasing the number of scans (to improve the signal-to-noise ratio) or magnetic field q-gradients (to get more points in the attenuation decay curve) would require an increase in the diffusion experiment time. We have verified that the structure is quenched in a particular state without noticeable stress relaxation within that 30 min delay in between each strain step. Since the structural transformations induced by the applied strain are metastable during the transition, a longer diffusion measurement would not allow the distinction or detection of any structural evolution.[60]

The sample preparation protocol for the study of the lamellae-to-onion transition was identical to that described for ^{2}H NMR imaging in section 2.3.1. After lamellar orientation at 42 °C (5 s^{-1} for 60 min), shear was stopped and the temperature was then decreased to 25 °C. The transition from planar lamellae to MLVs was again followed using a "start–stop" experiment where a certain shear rate was applied for a finite period of time followed by diffusion measurements without shear individually in each of the spatial directions until the transformation was completed. Experiments by Medronho *et al.*[57] indicated that the hypothetical cylindrical intermediate structure appears after 3000 strain units (for shear rate 5 s^{-1} this means t = 600 s) so it

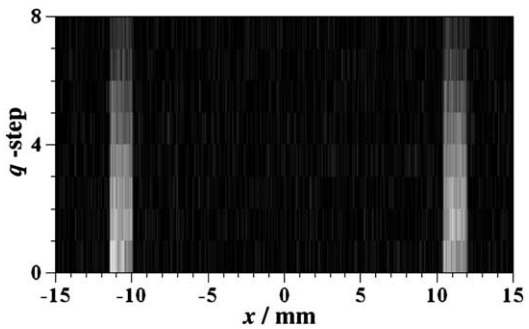

Fig. 6 1D intensity profiles after 1D FT of the NMR echo for the oriented planar lamellae before strain was applied (magnetic field q-gradient applied in velocity direction).

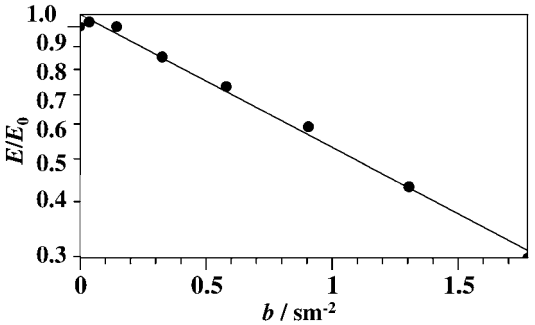

Fig. 7 Signal intensities as obtained by integration over the 1D profiles in Fig. 6. The slope of the fit yields the water self-diffusion coefficient, D_w.

was important to focus our study on the initial part of the process. A shear rate of 5 s^{-1} was applied for 60 s during the first 10 min (10 steps of 300 strain units). Then, two steps of 3000 strain units each were applied followed by a step of 9000 strain units and finally a step of 18000 strain units. Thus, the total strain was 36000 strain units which, under these conditions, is expected to be enough to complete the transition of planar layers into MLVs.

The opposite transition from MLVs to planar lamellae was followed in a similar way. MLVs were initially prepared at 36 °C at a constant shear rate of 5 s^{-1} during 1h. Then, shear was ceased and temperature increased to 42 °C. Since the process is even more rapid in this direction[57] we reduced the shear rate to 1 s^{-1} resulting in five initial strain steps of only 60 strain units each (each step takes 60 s). This was followed by one step of $\gamma = 100$, three steps of $\gamma = 200$, one step of $\gamma = 800$ and a final step of $\gamma = 1800$, resulting in a total strain of 3600. In between each strain step a diffusion measurement without shear, individually in each of the spatial directions, was performed.

3. Results and discussion

3.1 Spatial dependence of the transitions

3.1.1 Lamellae-to-onion transition. In Fig. 8 we present waterfall plots of five selected strains. Each individual plot represents the ^{2}H spectra as a function of the gap position. Initially, only planar lamellae are present with the typical splitted signal (doublet). Water molecules exchange rapidly with the locally isotropic bulk but since their diffusive motion is perturbed at the bilayer interface (at where they have a preferred orientation) a residual anisotropy is present giving rise to the observed quadrupolar splitting, $\Delta\nu_Q$.

With increasing strain, the line shape evolves in two ways; essentially the resonances are broadened and $\Delta\nu_Q$ decreases. While the former observation indicates that molecular reorientational motion is slow the latter indicates an increase of curvature in the system. Diffusion along curved layers is connected to an extra rotational component leading to an additional motional narrowing of the spectrum. As the transformation from planar lamellae to MLVs evolves, eventually all orientations of the interface normal with respect to the external magnetic field can be experienced and the residual anisotropy can be averaged to zero resulting in a collapse of the quadrupolar splitting and a broad single peak in the final MLV state. The data in Fig. 8 also

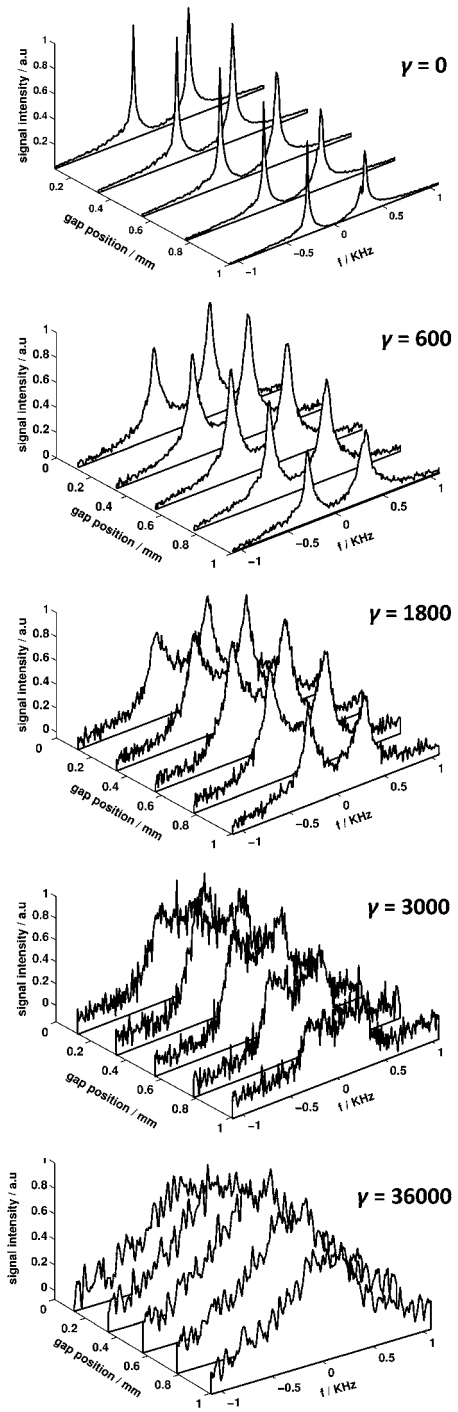

Fig. 8 Continuous transition from planar lamellae to MLVs. The deuterium spectra are shown as a function of the gap position (from the inner moving wall to the outer fixed wall) for five selected strains of 0, 600, 1800, 3000 and 36000. The temperature is 36 °C.

confirms that the transformation of planar lamellae into MLVs is continuous (no sudden changes in the spectra are observed) and spatially homogeneous (the strain dependent structural changes occur uniformly across the annular gap of the Couette cell). Such changes with strain are consistent with our previous results based on ^{2}H NMR without spatial resolution as published by Medronho *et al.*[57] In particular quadrupolar splittings $\Delta\nu_Q$ and NMR line widths as extracted from this study are in accordance to Medronho *et al.*[57] and discussed there in detail.

These results are in total agreement to the signal decay we observe with diffusion imaging for the lamellae-to-onion transition as shown, for instance in Fig. 6. The diffusion data were acquired before strain was applied and represent the signal decay as a function of magnetic field q-gradients applied in velocity direction. The signal attenuation is homogeneous across the gap indicating the diffusional behavior in the velocity direction is independent of the position in the sample. Similar images have been acquired in the gradient and vorticity directions, thus confirming by means of diffusion imaging (as an independent approach compared to ^{2}H NMR imaging) that the formation of onions is indeed a homogeneous process across the sample volume. There is no indication of vorticity banding as observed during the lamellae-to-onion transformation in the system SDS/dodecane/pentanol/water.[37]

3.1.2 Onion-to-lamellae transition. As one can observe from Fig. 9 the strain and spatially dependent spectra obtained during the onion-to-lamellae transition differs significantly from the reverse transition as discussed above in 3.1.1. Initially, the broad singlet from MLVs is observed uniformly across the annular gap of the Couette cell. The kinetics of the transition is in accordance with Medronho *et al.*[57] Very little strain is needed to promote the initial transition from MLVs to planar lamellae. Clearly, it is a spatially inhomogeneous process with a preferential nucleation of the aligned lamellar state (doublet) close to the inner rotating cylinder. With strain the boundary between planar lamellae and MLVs moves towards the outer stationary cylinder (along the velocity gradient direction). The discontinuous nature of the transition is obvious and confirms our hypothesis of a spatial coexistence of both structures within the gap as suggested by Medronho *et al.*[57]

The spatial resolution of the NMR image is restricted to 6 pixels across the gap, however, this is sufficient resolution to characterize the spatially inhomogeneous transition since the boundary between the onion and the planar lamellae state is not sharp. The transition region covers two to three pixels. This can be interpreted as a change of the density ratio between planar lamellae (near the rotating cylinder) and onions (near the stationary cylinder) after initial shear was applied. In this picture one may expect to find small amounts of onions or incomplete aligned layers even in regions mainly dominated by complete aligned planar lamellae. Correspondingly, small amounts of already disrupted structures may lead to the disturbance of regions still dominated by onions.

The coexistence of the onion and lamellar state separated in space should lead to distinct apparent diffusivities dependent on the position in the sample and the direction of molecular displacement. Diffusion imaging is suitable to measure the corresponding diffusion coefficients. In Fig. 10 we show the NMR signal attenuation as a function of the q-space magnetic field gradient applied in the vorticity, velocity and velocity gradient directions, respectively. We also indicate the boundary between the two states by black lines, which can be distinguished by means of the difference in signal attenuation.

The data set shown was obtained at 240 strain units. One clearly observes a stronger attenuation of the NMR signal near

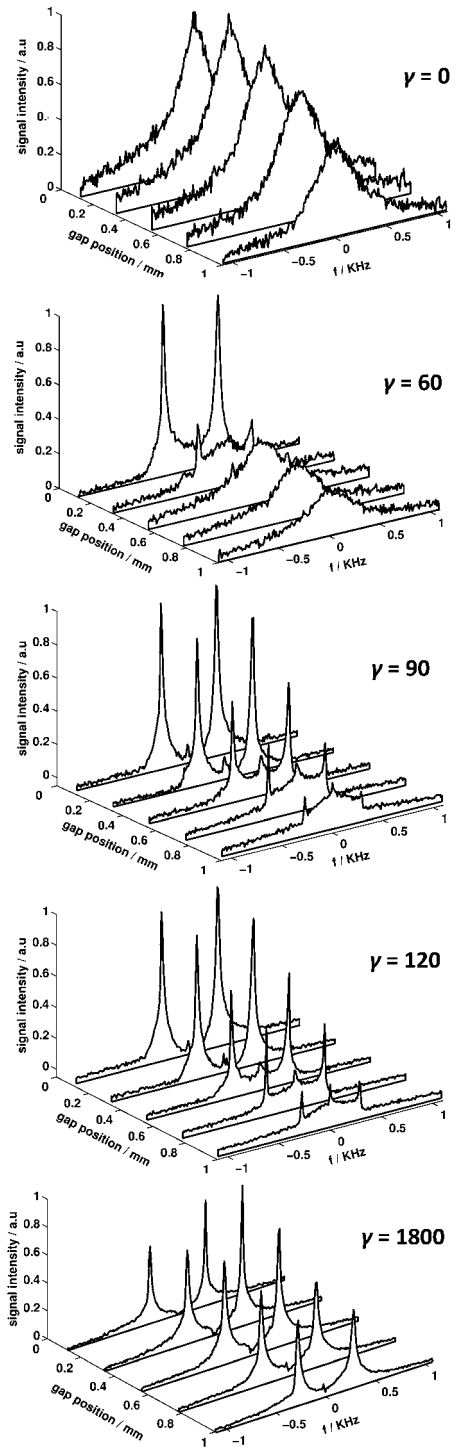

Fig. 9 Discontinuous transition from MLVs to planar lamellae. The deuterium spectra are represented as a function of the gap position (from the inner moving wall to the outer fixed wall) for five selected strains of 0, 60, 90, 120 and 1800. The temperature is 42 °C.

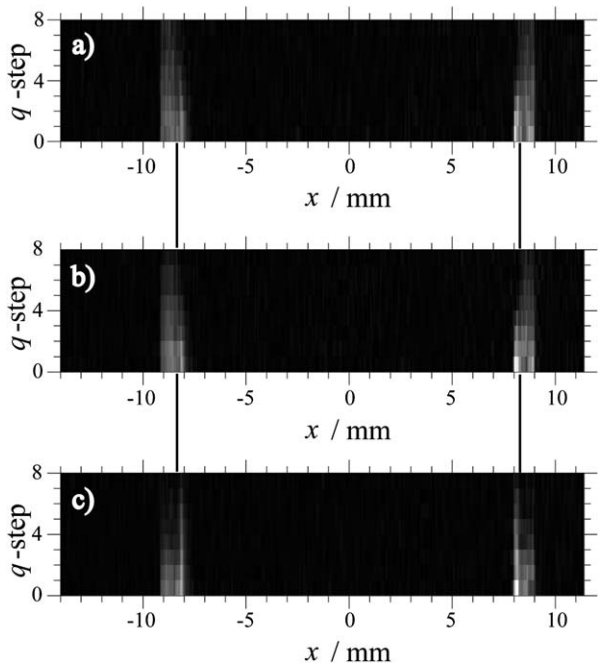

Fig. 10 1D Profiles across the cell obtained from diffusion imaging during the transition from MLVs to planar lamellae. Signal decays with increasing q-values are mapped for a) the vorticity b) velocity and c) velocity gradient direction at a strain of 240. The position of the boundary between the lamellae and onion state in each of the three directions is indicated by the black lines between the maps. See text for more details.

the inner wall in the vorticity and velocity direction (Fig. 10a and 10b), while the situation is opposite for the velocity gradient direction in Fig. 10c). Here the signal is hardly attenuated near the inner wall of the Couette cell despite the fact that the maximum applied q-space gradient (0.44 T m^{-1}) is more than twice as strong as compared to the q-gradients applied in the vorticity and velocity direction (0.2 T m^{-1}). One may easily attribute this small signal attenuation to the restricted diffusion perpendicular to the planar sheets of the lamellar state building up near the rotating part of the Couette cell. In contrast, diffusion paths are less obstructed along the plane of the lamellar sheets which leads to the observed stronger signal attenuation in vorticity and velocity direction near the inner Couette cell wall (see Fig. 10a and 10b).

More quantitatively, diffusion coefficients may be extracted for each pixel in the NMR image. One example in flow direction is shown in Fig. 11 for a strain of 240. Based on the obtained diffusivities it is now possible to determine the position of the interface between the onion and the planar lamellae by first calculating the averages of the diffusivities in both regions individually. We may then define the position of the interface to be at the point where the diffusivity reaches the intermediate value between these two averages. Similar maps may be obtained in the velocity gradient and the vorticity direction with coinciding positions of the interface in all three directions for each individual strain.

One may notice that diffusivities within the two regions in Fig. 11 differ slightly from those of the pure lamellar or onion states (see next subsection 3.2). We attribute that to already disrupted vesicles in the onion state leading to an increased diffusivity. Correspondingly, planar lamellae may not be completely aligned,[17,57,69] thus reducing the diffusion coefficient in flow direction. This is in agreement with the spectra in Fig. 9

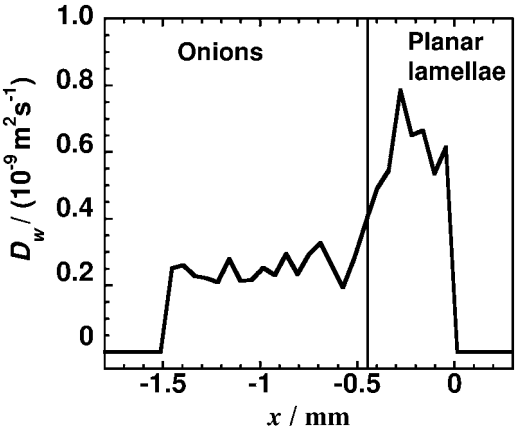

Fig. 11 Diffusion coefficients across the gap in flow direction extracted from NMR signal decays after an applied strain of 240. The position of the interface is indicated.

where features of onions can be seen at a gap position mainly occupied by planar lamellae and *vice versa*.

As is obvious from Fig. 11, diffusion imaging enables one to asses the inhomogeneous nature of the onion-to-lamellae transition. In Fig. 12 we plot the position of the interface as obtained by diffusion imaging (●). Independently, we determined the position of the interface from the ^{2}H NMR data as shown in Fig. 9 by fitting the spectra with Lorentzian functions (see also Medronho *et al.*[57]). The position of the interface (■ in Fig. 12) is subsequently interpolated where the integral over the two lamellar Lorentzian lines is equal to the integral over the one from the onion state.

A key feature of Fig. 12 is the propagation of the interface between onions and planar lamellae with strain, independent of the method used. Furthermore, ^{2}H NMR as well as diffusion imaging allow to conclude that the transition to perfectly aligned planar lamellae is not completed even at strains as high as 3600. This seems to be in contradiction to the last spectra in Fig. 9 at a strain of 1800 at a first glance. However, a detailed analysis reveals that the planar lamellae contribute less than 50% to the signal at the stationary wall, which is still dominated by a broad and very flat line.

The differences between the two NMR methods in determining the interface position may be due to the very different properties the two methods are based on. Considering the fact that we observe a gradual spatial transition rather than a sharp boundary, diffusional properties of water may not change at the same rate as compared to spatial orientation of lamellae.

3.2 Intermediate structure

It has been suggested that an intermediate structure is present during the transition from planar lamellae to MLVs.[59] This structure would be fully formed after 3000 strain units and manifests its existence by a narrow, but reproducible, plateau in a plot of viscosity *vs.* strain.[59] Furthermore, at such deformation, the small angle light and small angle neutron scattering patterns are consistent with either a multilayered cylindrical intermediate (MLC) or a "two-dimensional powder" of large domains.[59] From our previous work,[57] the "two-dimensional powder" state was ruled out.

Fig. 13 shows the evolution of water diffusivities with strain for the three spatial directions. Initially, as expected for the planar lamellae oriented with the layers parallel to the Couette wall, D_w in the gradient direction is more than one order of magnitude smaller than D_w in the velocity and vorticity directions where the value is close to the "free" water self-diffusion coefficient. When strain is increased a pronounced decrease in D_w in the vorticity direction is observed while D_w in the velocity direction remains almost constant (until 2000 strain units). At 3000 strain units we observe a plateauing of D_w in the vorticity direction to its final value while D_w in the velocity direction decreased slightly. These observations are consistent with the expected diffusion behavior for a cylinder-like structure oriented along the velocity direction. Meanwhile, D_w in the velocity gradient direction is only slightly increased, which can be explained by the introduction of curvature while the intermediate structure is being formed. Finally, when the transformation from planar lamellae to MLVs is completed, D_w in all directions is essentially the same. As previously discussed, this is expected for MLVs due to their spherical symmetry.

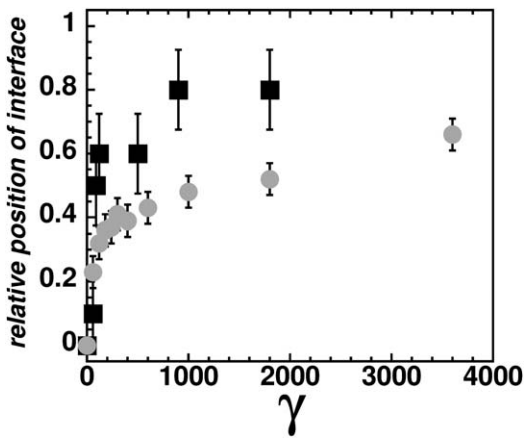

Fig. 12 Position of the interface as obtained from ^{2}H NMR imaging (■) and diffusion imaging (●) as a function of strain. The error bars indicate half the pixel size.

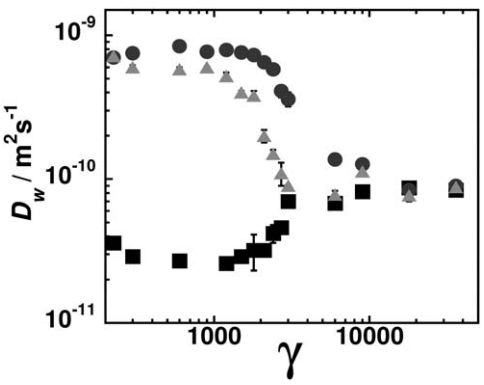

Fig. 13 D_w as a function of strain in gradient (■), vorticity (▲) and velocity direction (●) respectively. Temperature is 25 °C. The error bars (most of them are smaller than the symbol size) were obtained from the fitting procedure represented in Fig. 7.

The data are robust and allow us to unravel further details of the structural transformation. The diffusion has a high local anisotropy and the diffusion coefficient parallel to the layers is large enough that the water molecules diffuse for distances on the order of or larger than the characteristic size of the structure. For an observation time of 20 ms the mean square displacement is approximately 6.3 μm whereas the onion radius at a shear rate of 5 s^{-1} is about 5 μm.[88] Under these conditions cylinders and undulated structures can be distinguished. For cylinders, which are aligned along the velocity axis, we expect a large coefficient for diffusion parallel to the velocity direction and much smaller but equal values for diffusion parallel to the gradient and vorticity directions. For undulated structures diffusion parallel to the direction of the wave vector is slowed down due to the obstruction by the waves but still remains faster than diffusion perpendicular to the layers. Inspection of Fig. 13 shows $D_{velocity} > D_{vorticity} > D_{gradient}$ for strain values lower than 3000 which suggests undulations with a wave vector along the vorticity axis, in agreement with theoretical predictions[89,90] and molecular dynamics simulations.[91] Altogether, the diffusion results are consistent with the following pathway of onion formation: starting from flat layers, first an undulation with the wave vector along the vorticity axis is introduced. Eventually, undulations with wave vectors along the velocity directions are added. The fission and fusion of bilayer membranes occurs in an isotropic way such that initially cylinder-like structures are formed. These are, however, not perfectly straight along the velocity direction. Finally, further reorganization of membranes leads to the isotropic onion structure.

4. Conclusions

Shear-induced structural transitions in a lamellar $C_{10}E_3$ surfactant system were investigated. The continuous and homogeneous nature of the transition from planar lamellae to multilamellar vesicles (MLVs) and the discontinuous one, in the opposite direction, was confirmed by ^{2}H NMR and diffusion imaging. Moreover, during the transition from MLVs to planar lamellar structures, we proved that the nucleation and growth mechanism does not occur randomly and distributed over the whole sample, but starts from the inner moving Couette cell wall propagating towards the outer cylinder cell wall as strain increases. Both methods (^{2}H NMR and diffusion imaging) are in reasonable agreement regarding the position of the boundary between the two structures as a function of the applied strain in the case of the onion-to-lamellae transition.

Furthermore the properties of an intermediate structure formed during the homogeneous lamellae-to-onion transition as suggested by Zipfel *et al.*[59] were studied. We employed diffusion imaging to probe local anisotropy of the diffusive process as dependent on the applied strain. The obtained data support the picture of initial undulations followed by a cylinder-like intermediate structure oriented along the velocity direction during the continuous transition from planar lamellae to MLVs.

Acknowledgements

This work was supported by grants from the Swedish Research Council, the Swedish Foundation for International Cooperation in Research and Higher Education (STINT) and the New Zealand Foundation for Research Science and Technology. The Colloid Group in Coimbra University is supported by grants from the Fundação para a Ciência e Tecnologia (FCT) (projects ref: POCTI/QUI/45344/2002 and POCTI/QUI/58689/2004). BM thanks Fundação para a Ciência e tecnologia (FCT) (project ref. SFRH/BD/21467/2005). JB acknowledges the US NSF for fellowship funding. We thank Panos J. Photinos for inspiring discussions.

References

1 O. Diat and D. Roux, *J. Phys. II*, 1993, **3**, 9.
2 O. Diat, D. Roux and F. Nallet, *J. Phys. II*, 1993, **3**, 1427–1452.
3 O. Diat, D. Roux and F. Nallet, *J. Phys. IV*, 1993, **3**(C8), 193–204.
4 D. Roux, F. Nallet and O. Diat, *Europhys. Lett.*, 1993, **24**, 53.
5 F. Gauffre and D. Roux, *Langmuir*, 1999, **15**, 3070–3077.
6 A. Bernheim-Grosswasser, S. Ugazio, F. Gauffre, O. Viratelle, P. Mahy and D. Roux, *J. Chem. Phys.*, 2000, **112**, 3424–3430.
7 N. Mignet, A. Brun, C. Degert, B. Delord, D. Roux, C. Helene, R. Laversanne and J. C. Francois, *Nucleic Acids Res.*, 2000, **28**, 3134–3142.
8 P. Chenevier, B. Delord, J. Amédée, R. Bareille, F. Ichas and D. Roux, *Biochim. Biophys. Acta, Mol. Cell Res.*, 2002, **1593**, 17–27.
9 O. Regev, R. Backov and C. Faure, *Chem. Mater.*, 2004, **16**, 5280–5285.
10 A. Richard and L. Bourel-Bonnet, *Chem.–Eur. J.*, 2005, **11**, 7315–7321.
11 C. M. Douaihy, V. Koka, C. Mingotaud and F. Gauffre, *J. Colloid Interface Sci.*, 2006, **303**, 280–287.
12 M. Redkar, P. A. Hassan, V. Aswal and P. Devarajan, *J. Pharm. Sci.*, 2007, **96**, 2436–2445.
13 A. Bouter, B. Delord, E. Dransart, C. Poirier, L. Johannes and D. van Effenterre, *Biol. Cell*, 2008, **100**, 717–725.
14 C. Faure, M.-E. Meyre, S. Trépout, O. Lambert and E. Lebraud, *J. Phys. Chem. B*, 2009, **113**, 8552–8559.
15 F. Gauffre and D. Roux, *Langmuir*, 1999, **15**, 3738–3747.
16 D.-W. Kim, S.-G. Oh, S.-C. Yi, B.S.-Y. and S.-K. Moon, *Chem. Mater.*, 2000, **12**, 996–1002.
17 S. Müller, C. Börschig, W. Gronski, C. Schmidt and D. Roux, *Langmuir*, 1999, **15**, 7558–7564.
18 O. Diat, D. Roux and F. Nallet, *Phys. Rev. E: Stat. Phys., Plasmas, Fluids, Relat. Interdiscip. Top.*, 1995, **51**, 3296–3299.
19 P. Sierro and D. Roux, *Phys. Rev. Lett.*, 1997, **78**, 1496–1499.
20 T. D. Le, U. Olsson and K. Mortensen, *Phys. Chem. Chem. Phys*, 2001, **3**, 1310–1316.
21 J. Leng, F. Nallet and D. Roux, *Eur. Phys. J. E: Soft Matter Biol. Phys.*, 2001, **4**, 337–341.
22 A. S. Wunenburger, A. Colin, J. Leng, A. Arnéodo and D. Roux, *Phys. Rev. Lett.*, 2001, **86**, 1374–1377.
23 Y. Suganuma, M. Imai, T. Kato, U. Olsson and T. Takahashi, *Langmuir*, 2010, **26**, 7988–7995.
24 T. Gulik-Krzywicki, J. C. Dedieu, D. Roux, C. Degert and R. Laversanne, *Langmuir*, 1996, **12**, 4668.
25 P. Butler, *Curr. Opin. Colloid Interface Sci.*, 1999, **4**, 214–221.
26 W. Richtering, *Curr. Opin. Colloid Interface Sci.*, 2001, **6**, 446–450.
27 K. Mortensen, *Curr. Opin. Colloid Interface Sci.*, 2000, **6**, 140–145.
28 M. G. Berni, C. J. Lawrence and D. Machin, *Adv. Colloid Interface Sci.*, 2002, **98**, 217–243.
29 M. Gradzielski, *J. Phys.: Condens. Matter*, 2003, **15**, R655–R697.
30 L. Soubiran, C. Coulon, P. Sierro and D. Roux, *Europhys. Lett.*, 1995, **31**, 243.
31 J. Läuger, R. Weigel, K. Berger, K. Hiltrop and W. Richtering, *J. Colloid Interface Sci.*, 1996, **181**, 521.
32 J. Bergenholtz and N. J. Wagner, *Langmuir*, 1996, **12**, 3122–3126.
33 P. Panizza, A. Colin, C. Coulon and D. Roux, *Eur. Phys. J. B*, 1998, **4**, 65–74.
34 J. Zipfel, J. Berghausen, P. Lindner and W. Richtering, *J. Phys. Chem. B*, 1999, **103**, 2841–2849.
35 G. Fritz, N. J. Wagner and E. W. Kaler, *Langmuir*, 2003, **19**, 8709–8714.

36 L. Courbin, R. Pons, J. Rough and P. Panizza, *Europhys. Lett.*, 2003, **61**, 275–281.
37 G. M. H. Wilkins and P. D. Olmsted, *Eur. Phys. J. E*, 2006, **21**, 133–143.
38 Z. Yatabe, Y. Miyake, M. Tachibana, C. Hashimoto, R. Pansu and H. Ushiki, *Chem. Phys. Lett.*, 2008, **456**, 31–35.
39 Z. Yatabe, R. Hidema, C. Hashimoto, R. R. Pansu and H. Ushiki, *Chem. Phys. Lett.*, 2009, **475**, 101–104.
40 L. Soubiran, I. Staples, E. Tucker, J. Penfold and A. Creeth, *Langmuir*, 2001, **17**, 7988–7994.
41 J. Penfold, E. Staples, I. Tucker, J. Hubbard, L. Soubiran and A. Creeth, *Fibre Diffraction Review*, 2003, **11**, 68–74.
42 G. Montalvo, M. Valiente and A. Khan, *Langmuir*, 2007, **23**, 10518–10524.
43 M. Youssry, L. Coppola, I. Nicotera and C. Moán, *J. Colloid Interface Sci.*, 2008, **321**, 459–467.
44 M. Lukaschek, S. Müller, A. Hasenhindl, D. A. Grabowski and C. Schmidt, *Colloid Polym. Sci.*, 1996, **274**, 1–7.
45 R. Weigel, J. Läuger, W. Richtering and P. Lindner, *J. Phys. II*, 1996, **6**, 529.
46 T. D. Le, U. Olsson, K. Mortensen, J. Zipfel and W. Richtering, *Langmuir*, 2001, **17**, 999–1008.
47 T. Kato, K. Miyazaki, Y. Kawabata, S. Komura, M. Fujii and M. Imai, *J. Phys.: Condens. Matter*, 2005, **17**, S2923–2928.
48 K. Miyazaki, Y. Kosaka, Y. Kawabata, S. Komura and T. Kato, *J. Appl. Crystallogr.*, 2007, **40**, s332–s334.
49 Y. Kosaka, M. Ito, Y. Kawabata and T. Kato, *Langmuir*, 2010, **26**, 3835–3842.
50 Z. Yuan, S. Dong, W. Liu and J. Hao, *Langmuir*, 2009, **25**, 8974–8981.
51 J. Zipfel, J. Berghausen, G. Schmidt, P. Lindner, P. Alexandridis, M. Tsianou and W. Richtering, *Phys. Chem. Chem. Phys.*, 1999, **1**, 3905–3910.
52 J. Zipfel, P. Lindner, M. Tsianou, P. Alexandridis and W. Richtering, *Langmuir*, 1999, **15**, 2599–2602.
53 J. Zipfel, J. Berghausen, G. Schmidt, P. Lindner, P. Alexandridis and W. Richtering, *Macromolecules*, 2002, **35**, 4064–4074.
54 G. Schmidt, S. Müller, C. Schmidt and W. Richtering, *Rheol. Acta*, 1999, **38**, 486–494.
55 D. Burgemeister and C. Schmidt, *Prog. Colloid Polym. Sci.*, 2002, **121**, 95–100.
56 C. Oliviero, L. Coppola, R. Gianferri, I. Nicotera and U. Olsson, *Colloids Surf., A*, 2003, **228**, 85–90.
57 B. Medronho, S. Shafaei, R. Szopko, M. G. Miguel, U. Olsson and C. Schmidt, *Langmuir*, 2008, **24**, 6480–6486.
58 G. Porte, J.-F. Berret and J. L. Harden, *J. Phys. II*, 1997, **7**, 459–472.
59 J. Zipfel, F. Nettesheim, P. Lindner, T. D. Le, U. Olsson and W. Richtering, *Europhys. Lett.*, 2001, **53**, 335–341.
60 F. Nettesheim, J. Zipfel, U. Olsson, F. Renth, P. Lindner and W. Richtering, *Langmuir*, 2003, **19**, 3603–3618.
61 F. Nettesheim, U. Olsson, P. Lindner and W. Richtering, *J. Phys. Chem. B*, 2004, **108**, 6328–6335.
62 B. Medronho, S. Fujii, W. Richtering, M. G. Miguel and U. Olsson, *Colloid Polym. Sci.*, 2005, **28**, 317–321.
63 S. Fujii and W. Richtering, *Eur. Phys. J. E*, 2006, **19**, 139–148.
64 S. Koschorek, S. Fujii and W. Richtering, *Prog. Theor. Phys., Suppl.*, 2008, **175**, 154–165.
65 S. Koschoreck, S. Fujii, P. Lindner and W. Richtering, *Rheol. Acta*, 2009, **48**, 231–240.
66 B. Medronho, M. G. Miguel and U. Olsson, *Langmuir*, 2007, **23**, 5270–5274.
67 S. Fujii, S. Koschorek, P. Lindner and W. Richtering, *Langmuir*, 2009, **25**, 5476–5483.
68 L. Filipelli, B. Medronho, C. O. Rossi, M. G. Miguel and U. Olsson, *Mol. Cryst. Liq. Cryst.*, 2009, **500**, 166–181.
69 B. Medronho, C. Schmidt, U. Olsson and M. G. Miguel, *Langmuir*, 2010, **26**, 1477–1481.
70 M. Medronho, B. Rodrigues, M. G. Miguel, U. Olsson and C. Schmidt, *Langmuir*, 2010, **26**, 11304–11313.
71 M. Klinkenberg, P. Blümler and B. Blümich, *J. Magn. Reson., Ser. A*, 1996, **119**, 197–203.
72 E. Fischer and P. T. Callaghan, *Europhys. Lett.*, 2000, **50**, 803–809.
73 P. T. Callaghan, C. D. Eccles and Y. Xia, *J. Phys. E: Sci. Instrum.*, 1988, **21**, 820–822.
74 P. T. Callaghan and Y. Xia, *J. Magn. Reson.*, 1991, **91**, 326–352.
75 P. L. Hubbard, K. M. McGrath and P. T. Callaghan, *Langmuir*, 2006, **22**, 3999–4003.
76 P. L. Hubbard, K. M. McGrath and P. T. Callaghan, *J. Phys. Chem. B*, 2006, **2006**, 20781–20788.
77 A. Lutti and P. T. Callaghan, *Phys. Rev. E: Stat., Nonlinear, Soft Matter Phys.*, 2006, **73**, 011710.
78 A. Lutti and P. Callaghan, *J. Magn. Reson.*, 2006, **180**, 83–92.
79 A. Lutti and P. T. Callaghan, *J. Magn. Reson.*, 2007, **187**, 251–257.
80 A. Lutti and P. T. Callaghan, *Eur. Phys. J. E*, 2007, **24**, 129–137.
81 P. T. Callaghan, *Rep. Prog. Phys.*, 1999, **62**, 599–670.
82 H. A. Barnes, J. F. Hutton and K. Walters, *An Introduction to Rheology*, Elsevier, Amsterdam, 1989.
83 J. Seelig and W. Niederberger, *J. Am. Chem. Soc.*, 1974, **96**, 2069–2072.
84 P. T. Callaghan, *Principles of Nuclear Magnetic Resonance Microscopy*, Clarendon Press, Oxford, 1991.
85 P. D. Majors and A. Caprihan, *J. Magn. Reson.*, 1991, **94**, 225–233.
86 S. A. Rogers and P. T. Callaghan, *Rheol. Acta*, 2009, **48**, 735–745.
87 E. O. Stejskal, *J. Chem. Phys.*, 1965, **43**, 3597–3603.
88 I. Åslund, B. Medronho, D. Topgaard, O. Söderman and C. Schmidt, *J. Magn. Reson.*, 2011, **209**, 291–299.
89 A. G. Zilman and R. Granek, *Eur. Phys. J. B*, 1999, **11**, 593–608.
90 G. Auernhammer and H. R. Brand, *Phys. Rev. E: Stat. Phys., Plasmas, Fluids, Relat. Interdiscip. Top.*, 2002, **66**, 061707.
91 T. Soddemann, G. K. Auernhammer, H. Guo, B. Dünweg and K. Kremer, *Eur. Phys. J. E*, 2004, **13**, 141–151.